

# Self-assembly of densely packed and aligned bilayer ZnO nanorod arrays

L. Chow,<sup>1,2,a)</sup> O. Lupan,<sup>1,3</sup> H. Heinrich,<sup>1,2</sup> and G. Chai<sup>4</sup>

<sup>1</sup>Department of Physics, University of Central Florida, Orlando, Florida 32816, USA

<sup>2</sup>Department of Mechanical, Materials, and Aerospace Engineering, Advanced Materials Processing and Analysis Center, University of Central Florida, Orlando, Florida 32816, USA

<sup>3</sup>Department of Microelectronics and Semiconductor Devices, Technical University of Moldova, 168 Stefan cel Mare Blvd., MD-2004 Chisinau, Republic of Moldova

<sup>4</sup>Apollo Technologies, Inc., 205 Waymont Court, S111, Lake Mary, Florida 32746, USA

(Received 28 January 2009; accepted 23 March 2009; published online 21 April 2009)

We present a method of self-assembly of densely packed and aligned bilayer ZnO nanorod arrays in a hydrothermal synthesis process. The alkali hydrothermal environment first induced the growth of hydroxalcalitelike zincowoodwardite plates, which provide a lattice-matched surface for the self-assembly of ZnO nanorod arrays. The high packing density of the ZnO nanorod arrays demonstrates efficient nucleation and growth processes of ZnO on the zincowoodwardite. The interfacial phenomena involved in the growth of ZnO and self-assembly are discussed. The two-dimensional arrays of ZnO nanorods may find future applications in nanoelectronics and nanophotonics. © 2009 American Institute of Physics. [DOI: 10.1063/1.3118583]

Self-assembly of nanostructured building blocks into large ordered hierarchical heterostructures is important for bottom-up strategies in near-future nanotechnology applications.<sup>1-3</sup> Various self-assembled hierarchical heterostructures have been reported before.<sup>4-6</sup> The importance of one-dimensional ZnO nanorods has been recognized due to its excellent materials properties. The capability to synthesize large quantities of uniform ZnO nanorods has been reported by different groups.<sup>7-11</sup> Our work<sup>12-14</sup> demonstrated a fast, simple, and safe hydrothermal method for the growth of uniform ZnO nanorods. So far only a handful of authors reported on fabricating these ZnO nanorods into large densely packed and uniformly sized arrays.

Recently there were several reports of the self-assembly of ZnO nanorods on Zn–Al layered double hydroxide  $[\text{Zn}_{1-x}\text{Al}_x(\text{OH})_2][\text{CO}_3^{2-} \cdot n\text{H}_2\text{O}]$ .<sup>15</sup> Liu *et al.*<sup>16</sup> described the synthesis of ZnO/Zn–Al layered double hydroxide (LDH) hierarchical heterostructures using an Al substrate suspended in a  $\text{Zn}(\text{CH}_3\text{CO}_2)_2$  aqueous solution. Koh and Loh<sup>17</sup> used aluminum-coated silicon as a substrate to synthesize hydroxalcalitelike Zn–Al LDH in zinc acetate and ammonia water to grow self-assembled ZnO nanorods on Zn–Al LDH.

Here, we report a *template-free* solution growth self-assembly technique to synthesize bilayers of densely packed and aligned ZnO nanorod arrays. In this process, ultrathin hydroxalcalitelike zincowoodwardite,  $[\text{Zn}_{1-x}\text{Al}_x(\text{OH})_2] \cdot \text{SO}_4$  (Refs. 18 and 19) plates are first synthesized in the solution. The alignment of the self-assembled bilayer ZnO nanorods is a direct consequence of the heterogeneous epitaxial growth of ZnO [0001] nanorods on the zincowoodwardite plates.

In the synthesis process, 100 ml of 0.1–0.5 M zinc sulfate  $[\text{Zn}(\text{SO}_4) \cdot 7\text{H}_2\text{O}]$  was mixed with 100 ml of 0.001–0.005 M of aluminum sulfate  $[\text{Al}_2(\text{SO}_4)_3 \cdot 18\text{H}_2\text{O}]$  first. Then sodium hydroxide (2 M) was gradually added until the mixture solution become colorless/transparent. This aqueous complex solution was heated to a temperature of 85–95 °C for 15 min without any stirring. Then the heater was turned

off and the solution was allowed to cool to room temperature. The synthesized materials on the silicon substrate were removed from the solution, then were washed with deionized water and dried in a hot-air flux.

Zincowoodwardites are layered compounds with positively charged layers of  $\text{Zn}^{2+}$  and  $\text{Al}^{3+}$ . These compounds have been studied<sup>20</sup> as catalysts, anionic exchanges, and sorbents. When the supply of  $\text{Al}^{3+}$  ions is unlimited, the zincowoodwardite will continue to grow and form interpenetrating plates, as shown in Fig. 1(a). However, if the supply of  $\text{Al}^{3+}$  ions is limited, as  $\text{Al}^{3+}$  ions were consumed, the growth of zincowoodwardite flakes will stop and the ZnO nanorods will start to grow on the basal plane of zincowoodwardite, since the lattice spacing in the ZnO basal plane matches quite well with the lattice spacing in the zincowoodwardite basal plane.

A FEI 200 focused ion beam (FIB) system was used to prepare samples for transmission electron microscope (TEM) experiments from the freestanding ZnO nanorod assembly. The ZnO self-assembly sample was mounted on a copper grid. The TEM experiment was performed with a FEI F30 TEM operating at 300 kV. Raman spectra were obtained using an excitation source with 633 nm radiation from a helium neon laser. The laser power was varied from 0.5 to 4 mW. All Raman spectra were acquired at room temperature.

Figure 1(a) shows flakes of zincowoodwardite, which were produced when the  $\text{Al}^{3+}$  ions concentration is high in the mixture solution. Figure 1(b) shows a typical bilayer of densely packed and aligned ZnO nanorod arrays in a template-free solution growth technique. The ZnO nanorods are aligned with each other quite well and perpendicular to the zincowoodwardite middle layer, which is too thin to be visible at this magnification. The high packing density of the aligned ZnO nanorods demonstrates efficient nucleation and growth processes of ZnO on the zincowoodwardite, as both sides of the plate can act as nucleation sites for the aligned ZnO nanorods arrays.

Furthermore, the nanorods in the array all have similar diameters and lengths, as shown in Fig. 1(b). Each individual ZnO nanorod has an average radius of 50 nm and the length

<sup>a)</sup>Electronic mail: chow@mail.ucf.edu.

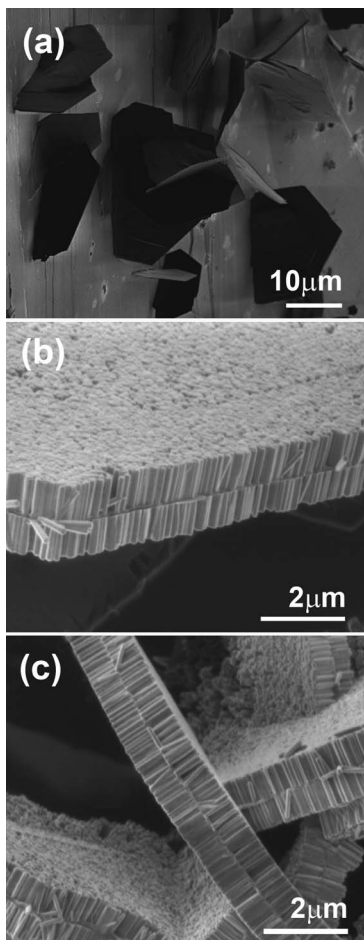


FIG. 1. SEM micrographs of (a) zincowoodwardite flakes, (b) bilayer of self-assembled, densely packed, and aligned ZnO nanorod arrays, and (c) several bilayers of densely packed and aligned ZnO nanorod arrays.

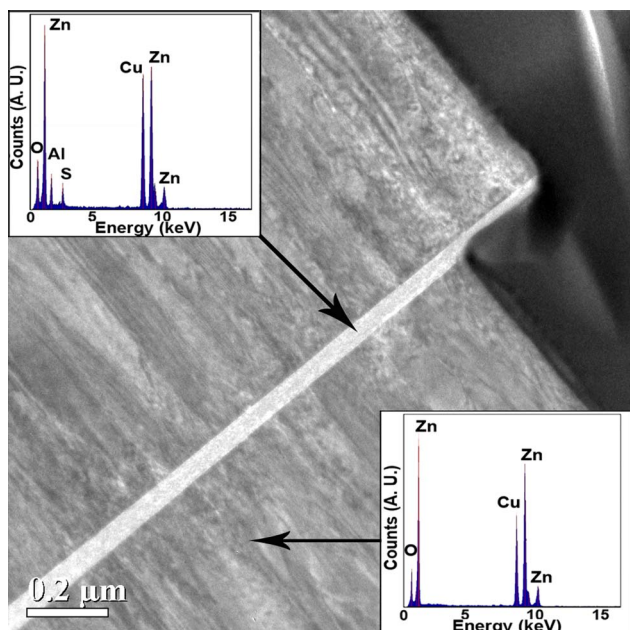


FIG. 2. (Color online) Cross-sectional TEM micrograph of the junction of the densely packed and aligned bilayer ZnO nanorod arrays showing the ultrathin zincowoodwardite plate. EDX spectrum of the zincowoodwardite plate is shown in the upper left corner, while the EDX spectrum of the aligned bilayer ZnO nanorods arrays is shown in the right lower corner.

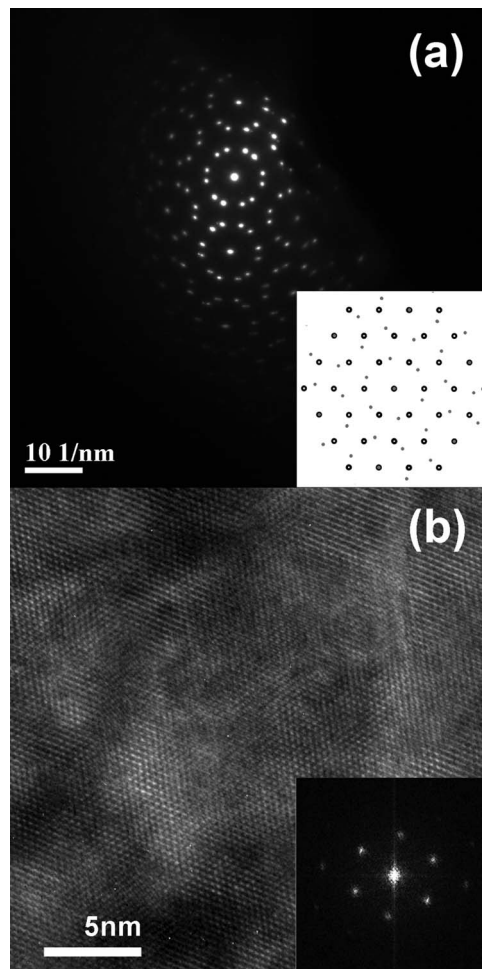


FIG. 3. (a) Small area electron diffraction pattern of aligned bilayer ZnO nanorod arrays, measured along the [0001] direction. Inset at lower right corner shows the arrangement of diffraction spots for a diffraction pattern along [0001] with two crystallographic domains rotated by 38.21° with respect to each other. (b) High-resolution TEM image of the ZnO nanorod viewed parallel to the rod *c*-axes. The inset at the right lower corner shows the SAED image from *one* individual nanorod along [0001] direction.

of the nanorod is about 700 nm. In Fig. 1(c), multiple bilayer structures of ZnO nanorod bundles are shown.

The controlled growth of individual, transferable units of the ZnO nanorod arrays on the  $[Zn_{1-x}Al_x(OH)_2] \cdot SO_4$  plate, as shown in Figs. 1(b) and 1(c), may be used as a freestanding, lasing array with highly oriented ZnO nanorods. Such densely packed and aligned arrays could also be used as potential photonic waveguide structures.

In order to investigate the growth mechanism of this self-assembled ZnO nanorod bilayer, TEM, and focused ion beam (FIB) are employed. The FIB technique has been used to fabricate ZnO nanorod devices by us in the past.<sup>21-23</sup> Here, FIB is employed to prepare a cross-sectional TEM sample. In Fig. 2, a TEM micrograph shows the zincowoodwardite plate sandwiched between two ZnO nanorod layers. The ultrathin zincowoodwardite plate has a thickness of about 60 nm. Some charging effect is seen on the zincowoodwardite plate indicating that it has a lower conductivity than the ZnO nanorods. The inset at the top left corner shows the energy dispersive x-ray (EDX) spectrum of the zincowoodwardite layer. We can see that Zn, Al, O, and S peaks are clearly present. The Cu  $K\alpha$  peak at 8 keV originates from the TEM Cu grid on which the sample was mounted. The inset at the

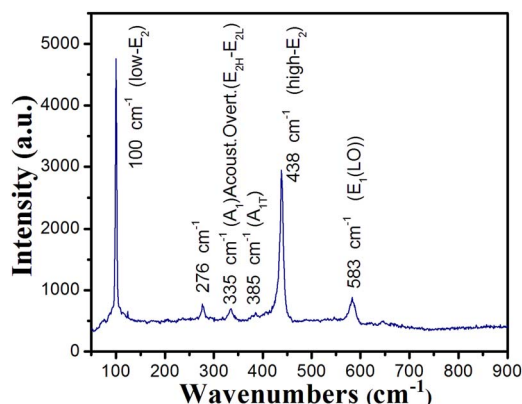


FIG. 4. (Color online) Raman spectrum of densely packed and aligned bilayer ZnO nanorod arrays measured at room temperature with a He–Ne laser with 2 mW input power.

lower right corner shows the EDX spectrum of the ZnO nanorods. It is clear that only Zn and O peaks are present. From Fig. 2, we can conclude that the densely packed ZnO nanorods grow perpendicular to the zincowoodwardite basal plane. Zincowoodwardite belongs to a family of layered compounds<sup>18–20</sup> with positively charged layers of  $\text{Zn}^{2+}$  and  $\text{Al}^{3+}$ , and interlayered charge balancing anions  $(\text{SO}_4)^-$ . It has a lattice constant of 3.076 Å in the basal plane which matches with the lattice constant of (0001) plane of the hexagonal ZnO crystal (3.249 Å) to within 5%. This provides a plane for the growth of ZnO [0001] nanorods.

In Fig. 3(a), the small-area electron diffraction (SAED) patterns reveal a hexagonal symmetry when the electron beam aligned parallel to the ZnO nanorod *c*-axis. The electron beam is spread over several nanorods, the diffraction pattern reveals not only the crystal structure and lattice parameters, but also orientation relations between these nanorods. It shows that  $\{2,1,-3,0\}$  diffraction spots from neighboring nanorods overlap, while  $\{0,1,-1,0\}$  and  $\{1,1,-2,0\}$  reflections from different nanorods are rotated with respect to each other. This corresponds to  $\Sigma 7$  grain boundaries and rotations of  $38.21^\circ$  about the *c*-axis for crystal lattices in neighboring nanorods. The inset at the lower right corner shows a simulated diffraction spots for a diffraction pattern along [0001] with two crystallographic domains rotated by  $38.21^\circ$ . In Fig. 3(b) a high-resolution TEM image of the ZnO nanorods reveals that they are high-quality single crystals without defects. The inset in Fig. 3(b) shows the SAED image from one individual nanorod along [0001] direction.

To demonstrate the optical quality of these densely packed ZnO arrays, we carried out Raman measurements using a He–Ne laser. Figure 4 shows Raman spectrum of ZnO nanorod arrays. It can be seen that the dominant peaks at  $100\text{ cm}^{-1}$  and  $438\text{ cm}^{-1}$  are attributed to the low- and high- $E_2$  mode of nonpolar optical phonons,<sup>24</sup> respectively. The  $E_2$  mode<sup>25</sup> has a width of  $11\text{ cm}^{-1}$ , indicating a good crystal quality of the self-assembled ZnO nanorod-bundle structures. The peak at  $335\text{ cm}^{-1}$  is attributed to the second-order nonpolar Raman processes, while that at  $385\text{ cm}^{-1}$  corresponds to  $A_1$  transverse optical (TO) mode.<sup>26</sup> The  $E_1$  (LO) phonon mode can be observed at  $583\text{ cm}^{-1}$  when the *c*-axis of wurtzite ZnO is perpendicular to the sample surface.<sup>27</sup> However, the  $583$  and  $275\text{ cm}^{-1}$  peaks can be

attributed to the electric field induced Raman modes as were observed<sup>28</sup> previously.

In conclusion, a self-assembly technique was developed for the growth of densely packed and aligned ZnO nanorod arrays in a hydrothermal process. Well-aligned bilayers of ZnO nanorod arrays were synthesized through the formation of a thin layer of hydrotalcite-like zincowoodwardite. The zincowoodwardite plates provide an oriented growth of self-assembled densely packed and aligned ZnO nanorod arrays. This process provides a simple and reproducible fabrication method for the growth of well-aligned ZnO nanorod arrays, which could be of use in the future for the fabrication of photonic devices.

This work was made possible in part through grants from Apollo Technology, Inc., Florida High Tech Corridor Research Program and U.S. Department of Agriculture. The authors would like to acknowledge micro-Raman measurements provided by S. Park and A. Schulte.

- <sup>1</sup>X. Wang, J. Zhuang, Q. Peng, and Y. Li, *Nature (London)* **437**, 121 (2005).
- <sup>2</sup>A. Aggeli, I. A. Nyrkova, M. Bell, R. Harding, L. Carrick, T. C. B. McLeish, A. N. Semenov, N. Boden, *Proc. Natl. Acad. Sci. U.S.A.* **98**, 11857 (2001).
- <sup>3</sup>K. Ariga, T. Nakanishi, and J. P. Hill, *Curr. Opin. Colloid Interface Sci.* **12**, 106 (2007).
- <sup>4</sup>Y. N. Xia, J. A. Rogers, K. E. Paul, and G. M. Whitesides, *Chem. Rev. (Washington, D.C.)* **99**, 1823 (1999).
- <sup>5</sup>S. A. Jenekhe and X. L. Chen, *Science* **279**, 1903 (1998).
- <sup>6</sup>M. Reches and E. Gazit, *Science* **300**, 625 (2003).
- <sup>7</sup>X. D. Wang, C. J. Summers, and Z. L. Wang, *Nano Lett.* **4**, 423 (2004).
- <sup>8</sup>L. Vayssieres, *Adv. Mater. (Weinheim, Ger.)* **15**, 464 (2003).
- <sup>9</sup>C. Pacholski, A. Kornowski, and H. Weller, *Angew. Chem., Int. Ed.* **41**, 1188 (2002).
- <sup>10</sup>W. I. Park, D. H. Kim, S. W. Jung, and G. C. Yi, *Appl. Phys. Lett.* **80**, 4232 (2002).
- <sup>11</sup>B. Liu and H. C. Zeng, *J. Am. Chem. Soc.* **125**, 4430 (2003).
- <sup>12</sup>O. Lupan, L. Chow, G. Chai, B. Roldan Cuenya, A. Naitabdi, S. Park, A. Schulte, and H. Heinrich, *Mater. Sci. Eng. B* **145**, 57 (2007).
- <sup>13</sup>O. Lupan, L. Chow, G. Chai, A. Schulte, S. Park, O. Lopatiuk-Tirpak, L. Chernyak, and H. Heinrich, *Superlattices Microstruct.* **43**, 292 (2008).
- <sup>14</sup>D. Polsongkram, P. Chamminok, S. Pukird, L. Chow, O. Lupan, G. Chai, H. Khallaf, S. Park, and S. Schulte, *Physica B* **403**, 3713 (2008).
- <sup>15</sup>F. Thevenot, R. Szymanski, and P. Chaumette, *Clays Clay Miner.* **37**, 396 (1989).
- <sup>16</sup>J. Liu, X. Huang, Y. Li, K. M. Sulieman, X. He, and F. Sun, *J. Phys. Chem. B* **110**, 21865 (2006).
- <sup>17</sup>Y. W. Koh and K. P. Loh, *J. Mater. Chem.* **15**, 2508 (2005).
- <sup>18</sup>T. Witzke and G. Raade, *Neues Jahrb. Mineral., Monatsh.* **2000**, 455.
- <sup>19</sup>P. S. Braterman, Z. P. Xu, and F. Yarberry, in *Handbook of Layered Materials*, edited by S. M. Auerbach, K. A. Carrado, and P. K. Dutta (Dekker, New York, 2004), pp. 373–474.
- <sup>20</sup>V. Rives, *Layered Double Hydroxides: Present and Future* (Nova Science, New York, 2001).
- <sup>21</sup>O. Lupan, L. Chow, G. Chai, L. Chernyak, O. Lopatiuk, and H. Heinrich, *Phys. Status Solidi A* **205**, 2673 (2008).
- <sup>22</sup>O. Lupan, G. Chai, and L. Chow, *Microelectron. Eng.* **85**, 2220 (2008).
- <sup>23</sup>O. Lupan, L. Chow, G. Chai, and H. Heinrich, *Chem. Phys. Lett.* **465**, 249 (2008).
- <sup>24</sup>Y. J. Xing, Z. H. Xi, Z. Q. Xue, X. D. Zhang, J. H. Song, R. M. Wang, J. Xu, Y. Song, S. L. Zhang, and D. P. Yu, *Appl. Phys. Lett.* **83**, 1689 (2003).
- <sup>25</sup>T. C. Damen, S. P. S. Porto, and B. Tell, *Phys. Rev.* **142**, 570 (1966).
- <sup>26</sup>J. M. Calleja and M. Cardona, *Phys. Rev. B* **16**, 3753 (1977).
- <sup>27</sup>J. F. Scott, *Phys. Rev. B* **2**, 1209 (1970); R. Zhang, P. G. Yin, N. Wang, and L. Guo, *Solid State Sci.* **11**, 865 (2008).
- <sup>28</sup>M. Tzolov, N. Tzenov, D. Dimova-Malinovska, M. Kalitzova, C. Pizzuto, G. Vitali, G. Zollo, and I. Ivanov, *Thin Solid Films* **379**, 28 (2000).